INTERNATIONAL JOURNAL OF ENGINEERING SCIENCES & MANAGEMENT

Structural, optical and luminescent properties of MgO: Mn2+ nanophosphors prepared by facile combustion route

P.B Devaraja[*1], H. Nagabhushana[2], S.C. Prashantha[3], C. Vedamurthy[1] and M.C.Kirankumar[1]
[1]Department of Physics, Kalpataru institute of Technology, Tiptur-572201, India
[2]Prof. CNR Rao center for advanced materials, Tumkur University, Tumkur-572103, India
[3]Research center, Department of Science, East West Institute of Technology, Bangalore-560091, India

ABSTRACT

A series of MgO:Mn2+ (1 to 9 mol%) phosphors were synthesized by solution combustion route at ~ 400oC using glycine as fuel. The nanophosphors were well characterized by powder X-ray diffraction (PXRD), scanning electron microscopy (SEM) PXRD results confirmed the single pure cubic phase of the prepared samples and SEM micrographs indicate that the powder was highly porous and agglomerated. Upon excitation at 370 nm, an intense a blue emission at 405 nm owing to the 3B1u1Ag transition of Mn2+ ions the maximum PL intensity of the phosphor was recorded at 3 mol% and then it decreases due to concentration quenching. The Commission International De I-Eclairage chromaticity co-ordinates (CIE) and CCT (correlated color temperature) values indicate that MgO: Mn2+ phosphor was quite useful for the display devices and also for solid state lighting.

Keywords: MgO:Mn2+, nanophosphor, Photoluminescence.

1. Introduction

Now a day's many studies have focused on nanomaterials due to their unique optical electronic, thermal, chemical and mechanical properties. Indeed, the synthesis of nanomaterials becoming increasingly attractive in technology. In the past decade nano sizedmaterials have been extensively investigated due to their attractive size-dependent properties. Great interest has been paid specifically to semiconductor nano crystals which often exhibit strong variations in their properties with size as a consequence of the quantum size effect [1,2].

Preparation of nanomaterials with controlled particle shape and size has been found to be of great importance for tailoring desired material properties. Furthermore, the luminescent properties of oxide based inorganic phosphors have been extensively investigated. Among the oxide material, MgO was useful in many technological applications in particular for fluorescent lamps, plasma display panels due to its high luminescence efficiency and chemical stability [3] and it has attracted interest as a semiconductor of a wide energy band gap (~ 7.8 eV) applicable for various ultraviolet photoelectronic devices [4], and also as a phosphor host material [5]. When doped with Co^{2+}, Mn^{2+} or rare earth cations, exhibit luminescence and can be used as a cathode luminescent material [6].

Transition metal (TM) ion forms an ideal active center mainly due to the possibility of its tuning over a wide emission wavelength ranging from green to orange and eventually to red by appropriately modifying thecrystal field of the hosts where the Mn^{2+} ions are located [7].

2. Experimental

Samples preparation:

Various concentrations of (1–9 mol %) Mn^{2+} ions activated MgO phosphors were prepared by solution combustion method. Aqueous solution containing stoichiometric amounts of analar grade magnesium nitrate [$Mg(NO_3)_2$ $6H_2O$ (A.R)] as an oxidizer, glycine [NH_2CH_2COOH (A.R)] as a fuel and different molar concentration of Manganese(Mn) nitrate. The stoichiometry of the composition was calculated based on the total oxidizing and reducing valences of oxidizer and the fuel. The experimental process was performed by dissolving the above reagents together in a minimum amount of deionized water and the concentration of the Mn^{2+} ions was varied in the range 1-9 mol% in relation to Mg content. After mixing the starting materials placed in a Petri dish was then introduced into a muffle furnace at ~ 400 ºC for 5 min. As the ignition occurred, the reaction went on vigorously for a few seconds. Fluffy product was obtained after the combustion reaction [8].

Characterization:

The crystalline nature of the powder samples was characterized by powder X-ray diffraction (PXRD) using Shimadzu X-ray diffractometer (operating at 50 KV and 20 mA by means of Cu-K$_\alpha$ (1.541Å) radiation with a nickel filter at a

scan rate of 2 $^\circ$ min^{-1}). The surface morphology of the product was examined by Scanning Electron Microscopy (SEM) Hitachi table top (Model TM 3000). Transmission Electron Microscopy (TEM) analysis was performed on a (JEOL JSM 2100) (accelerating voltage up to 200 kV, LaB$_6$ filament). Fourier transform infrared spectroscopy (FTIR) studies of the samples were performed with a Perkin Elmer FTIR spectrophotometer. Photoluminescence studies were made using Horiba, (model fluorolog-3) spectrofluorimeter at RT using 450 W xenon as excitation source and Fluor Essence™ software was used for spectral analysis.

3.   Results and Discussion

Fig.1 shows the PXRD pattern of MgO: Mn^{2+} (1-9 mol %) nanophosphors. As can be seen from the PXRD studies a pure single cubic phase was obtained without calcined the product.
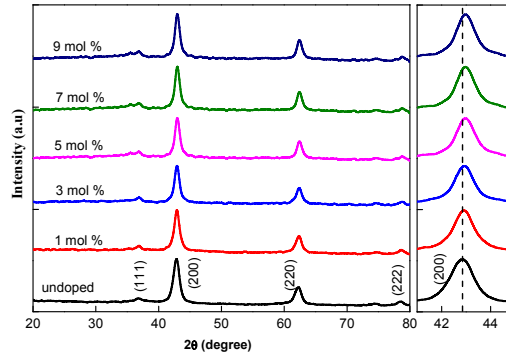

Fig.1. PXRD patterns of Mn^{2+} doped MgO.

Further, all the X-ray diffraction peaks of the samples at (111), (200), (220), (311), (222) were indexed well and matched with JCPDS card No. 4–829 and belongs to a space group *fm-3m* (225) [2]. The Mn^{2+}ions doped into MgO matrix causes expansion of the unit cell resulting in tensile stress, as a result the PXRD peaks shifted towards higher angle side [9]. The full width at half maximum (FWHM) of the diffraction peaks can be used to calculate the average crystallite size using Debye- Scherrer's formula [10] and it was found to be ~ 5-15 nm.

The average crystallite size (D) of the sample was estimated using Scherrer's formula $D = K\lambda/\beta\cos\theta$[10], where, k; the wavelength of X-rays (1.54 Å) used,θ;the Bragg's angle, K;the shape factor (0.9 for spherical particle, and β; the full width at half maxima (FWHM) in radian.

The room temperature Fourier transforms infrared (FTIR) spectra of undoped and MgO: Mn^{2+}(1–9 mol %) phosphors was shown in Fig. 2. The strong band at 438 cm^{-1} was associated with the characteristic vibrational mode of symmetric MgO$_6$ octahedral of MgO. Further, the peaks at 550-890 cm^{-1} (γ_1) were due to higher frequency of MgO stretching and 410-450 cm^{-1}(γ_2) was lower frequency stretching. The peak at 878 cm^{-1} was attributed to Mg-O-Mg interactions. The absorption in the range of 1300-1800 cm^{-1} related to hydroxyl group of molecular water at   1635 cm^{-1} , NH$_3$ at 1440 cm^{-1} and it was due to C=O stretching mode. The peak at ~2376 cm^{-1} arises due to absorption of atmospheric CO$_2$ on the metallic cations. Also, the absorption at ~3458 cm^{-1} indicate the presence of hydroxyl groups (O-H mode), which was probably due to the fact that the spectra were not recorded in situ and some water re-adsorption from the ambient atmosphere as occurred [11].
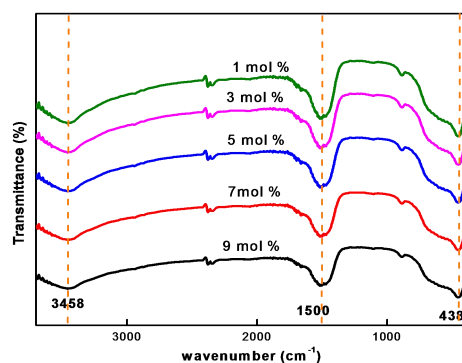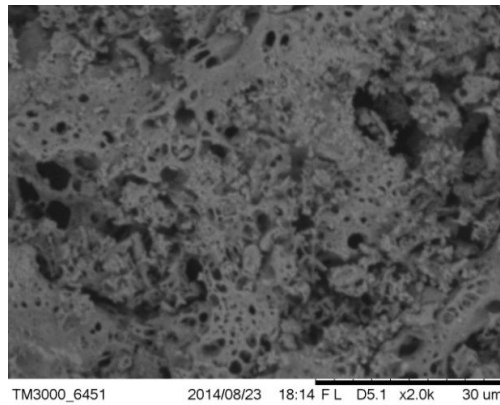

Fig.2.FT-IR spectra of un-doped and (1-9   mol %) Mn^{2+}doped MgO.

Texture, topography and surface features of the nanophosphors were studied by SEM and shown in Fig.3 .

Fig.3. SEM images of 1 mol % Mn²⁺doped MgO.

It was clearly observed from SEM pictures of MgO: Mn^{2+} (1 mol %) samples prepared via combustion technique. The powders shows porous and large agglomerates of very fine particles. Further, it was well known that, combustion synthesis reaction was influenced by metal–ligand complex formation. Depending upon the type of fuel and metal ions, the nature of combustion differs from flaming (gas phase) to non-flaming (smoldering and heterogeneous) type. Generally, flaming reactions involve liberation of large quantity of gas. The pores and voids were attributed to the large amount of gases escaping out of the reaction mixture during combustion [12].

Photoluminescence (PL) emission spectra of the MgO: Mn^{2+} phosphor was shown in Fig. 4.

The different atomic percentages Mn^{2+} doped MgO were measured with an excitation wavelength of 370 nm. The PL bands for the samples were not due to the band gap emission, but can be attributed to various structural defects. Further, these emissions would induce the formation of new energy levels in the band gap of MgO. Therefore, in spectrum of pure MgO a broad emission band observed at 405 nm was arising due to $^3B_{1u} \rightarrow {}^1A_g$ transition of the F_2^{2+} centre in D_{2h} symmetry [13]. Several additional bands centered at around 454, 486 and 503 nm which arise due to energy levels created with various F type anion vacancies. The emission bands were considerably blue shifted as the Mn^{2+} doping percentage was increased. This can be attributed to the increased density of surface defect states because of reduced crystallites size. The blue light emission bands at around 405 nm may originate from the recombination of the photo generated hole with an electron occupying the oxygen vacancy [14]. The green emission bands at around 503 nm may arise from the emission due to the oxygen ion vacancies (excited F centers) [15].
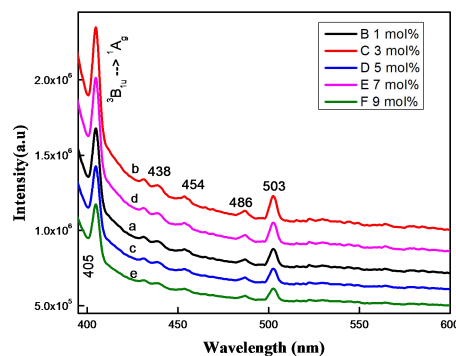
Fig.4. Emission spectra of MgO: Mn²⁺(1-9 mol %) (Excited at 370 nm).

MgO was an insulator, has high physical and chemical stability, poor desiccant, due to its high melting point used as a refractory etc. Also, it was used as a reference white color owing to its good diffusing and reflectivity properties [16]. MgO has a rock salt structure (fcc) with magnesium ions occupying octahedral sites within the anion

closed packed structure. Its ionic constituents comprise a relatively small number of electrons, its nanostructures were expected to have novel properties superior to their bulk counterparts due to the large surface to volume ratio effect of nanocrystals [17]. The Mg atoms were present at the corner of the cube and are coordinated by eight equivalent-nearest neighbor oxygen atoms. In this lattice, the point group symmetry of Mg sites in the cubic MgO structure was ideally D_{2d} and Mg site possesses inversion symmetry. When Mn^{2+} ions were doped into the host, they could probably occupy these sites. Owing to the different charge for the cations, oxygen vacancies were formed to balance the charge difference. The excess amount of Mg_2O_3 will likely reside on either surface or grain boundaries of the nanocrystals to yield optimum strain relief. The defect reaction equation can be represented in the following way,

$$(1-x)MgO + 0.5xMn_2O_3 = xDy'_{Ce} + 0.5x\,V_O^{\cdot\cdot} + (1-x)Mg_{Mg}^x + (2-0.5x)O_O^x \; ----(1)$$
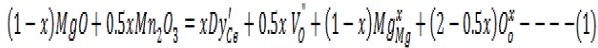
where 'Mn'_{Ce}' means 'Mn' occupying the site normally occupied by a 'Mg^{2+}' due to replacement by 'Mn', '$V_O^{\cdot\cdot}$' was the 'O^{2-}' vacancy, 'Mg_{Mg}^x' represents the rest magnesium in the lattice of MgO, and 'O_O^x' was the oxygen in the lattice of MgO [18].

To optimize the doping concentration for efficient luminescence, the concentration of Mn^{2+} ions in MgO phosphor was varied from 1 to 9 mol %. The variation of PL intensity with Mn^{2+} concentration was shown in Fig. 5. As can be seen from the figure, the luminescence intensities at 405 nm of the MgO: Mn^{2+} phosphors increases with the increase of Mn^{2+} ion concentration, reaches a maximum for 3 mol % of Mn^{2+} and then decreases with further increase of concentration due to energy transfer among the excited Mn^{2+} ions at higher concentrations and also due to concentration quenching. As dopant concentration of Mn^{2+} increases, $^3B_{1u} \rightarrow {}^1A_g$ transition dominates and the emission intensity increases. This may be attributed to the increase distortion of the local field around the Mn^{2+} ions. Also, when the concentration of Mn^{2+} continues to increase, the interaction between the dopant ions increases, leads to self-quenching and thereby PL intensity decreases [19].
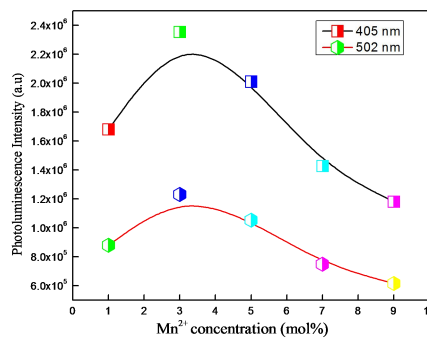

Fig.5. Photoluminescence intensity by MgO: Mn^{2+}(1-9 mol %) concentration.

The concentration quenching might be explained on the basis of following two factors: (i) the excitation migration due to resonance between the activators was enhanced when the doping concentration was increased, and thus the excitation energy reaches quenching centers, and (ii) the activators were paired or coagulated and were changed to quenching centers. The energy can also be transferred non-radiatively by the radiative reabsorption or multipole-multipole interaction [20]. Also, the increase in Mn^{2+} concentration can result in cross-relaxation processes in close $Mn^{2+} - Mn^{2+}$ pairs, the quenching of Mn^{2+} luminescence often occurs at low concentration.

The energy transfer mechanism in phosphors was essential in order to obtain the critical distance (Rc) i.e. the critical separation between Mn^{2+} and the quenching site was calculated according to the equation given by Blasse [21]

$$R_c \approx 2\left[\frac{3V}{4\pi X_c N}\right]^{1/3} \; -----(2)$$

where X_c; the critical concentration, N; the number of cation sites in the unit cell, and V; the volume of the unit cell. For MgO: Mn^{2+} nanophosphor the values of N,V and Xc were, 4, 74.78 $Å^3$ and 0.03 respectively. Using these parameters, the estimated 'R_c' was found to be 10.59 Å. Since 'R_c' was not less than 5Å, exchange interaction was not responsible for non radiative energy transfer process from one Mn^{2+} ion to another Mn^{2+} ion in this host. According to Blasse theory [22], the non radiative transfer between different Mn^{2+} ions in MgO phosphor may occur by radiative re-absorption/exchange interaction/ multipole-multipole interaction.

Therefore, multipolar interaction was used to explain the concentration quenching mechanism. Multipolar interaction involves several types of interaction such as dipole-dipole (d-d), dipole-quadrupole (d-q), quadrupole-quadrupole (q-q) interaction. As a result, the energy transfer process of Mn^{2+} in MgO phosphor would be due to multipolar interaction [5]. In order to determine the type of interaction involved in the energy transfer Vanuitert's [23] proposed an equation:

$$\frac{I}{X} = k\left[1 + \beta(X)^{Q/3}\right]^{-1} ----- (3)$$

where I; the integral intensity of emission spectra from 450-740 nm, X; the activator concentration, I/X; the emission intensity per activator (X), β and K ; constants for a given host under same excitation condition. According to above equation, Q=3 for the energy transfer among the nearest neighbor ions, while Q = 6, 8 and 10 for d-d, d-q and q-q interactions respectively [1]. Assuming that $\beta(X)^{Q/3} \gg 1$, above equation can be written as

$$\log\left(\frac{I}{X}\right) = K' - \left(\frac{Q}{3}\right)\log X \quad (K' = \log K - \log \beta) ----- (4)$$

From equation (11), the multipolar character (Q) can be obtained by plot log (I/X) v/s log (X) as shown in Fig. 6. The slope and multipolar character Q was found to be ~ -1.10697 and 6.2889 which was close to 6. Therefore, the concentration quenching in MgO: Mn^{2+} phosphor occurred due to dipole to dipole interaction.

Further, the intensity ratio of ED and MD (Asymmetry ratio, A_{21}) transitions were used to measure the symmetry of the local environment of the trivalent 4f ions which was sensitive to the nature of the Mn^{2+} ions in the host lattice [24]. This gives a measure of the degree of distortion from inversion symmetry of the local environment surrounding the Mn^{2+} ions in the host matrix.

Mn^{2+} (1-9 mol %) nanophosphors.

$$A_{21} = \frac{\oint I_2 \lambda_{405}}{\oint I_1 \lambda_{502}} ----- (5)$$

Where I_2; intensity at 405 nm and I_1; intensity at 502 nm. The values of A_{21} decrease with increase of Mn^{2+} ions. However, it was reasonable to believe that the doping of Mn^{2+} will introduce lattice defects, which will undoubtedly reduce the symmetry strength of the local environment of Mg^{2+} sites [25]. Consequently, the symmetry ratio of the sample doped with rare earth cations decreases with the increase of dopant concentration and as shown in Fig.7.
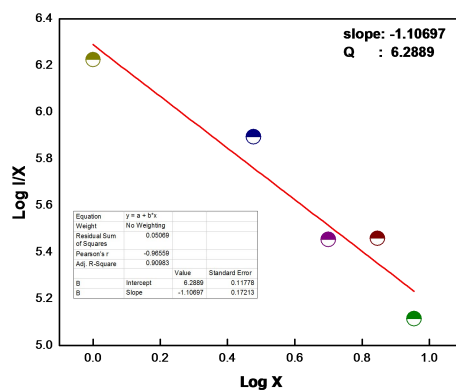

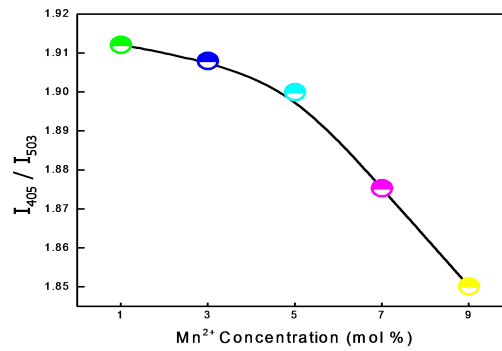*Fig.6. Relation between log(x) and log (I/x) in MgO:*

.

Fig.7. The effect of Mn²⁺ on the 405 nm emission peak and variation of asymmetric ratio with Mn²⁺ concentration.

The Commission International De I-Eclairage (CIE) chromaticity coordinates [26] for MgO: Mn^{2+} (1-9 mol %) phosphors was calculated as a function of Mn^{2+} concentration (Fig. 8(a)). The CIE coordinates of white emission of Mn^{2+} ions not only depend upon the asymmetric ratio but also depend upon the higher energy emission levels. Coordinated color temperature can be estimated by Planckian locus, which was only a small portion of the (x, y) chromaticity diagram and there exist many operating points outside the Planckian locus. If the coordinates of a light source do not fall on the Planckian locus, the correlated color temperature (CCT) was used to define the color temperature of a light source. CCT was calculated by transforming the (x, y) coordinates of the light source to (U', V') by using following equations, and by determining the temperature of the closest point of the Planckian locus to the light source on the (U', V') uniform chromaticity diagram (Fig. 8(b)) [27].

$$U' = \frac{4x}{-2x + 12y + 3} \ - - - - - (6)$$

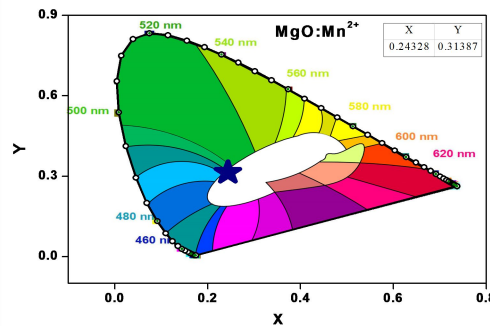$$V' = \frac{9y}{-2x + 12y + 3} \ - - - - - (7)$$

Fig 8(a). CIE chromaticity diagram of MgO: Mn²⁺ (3 mol %) nanophosphor.
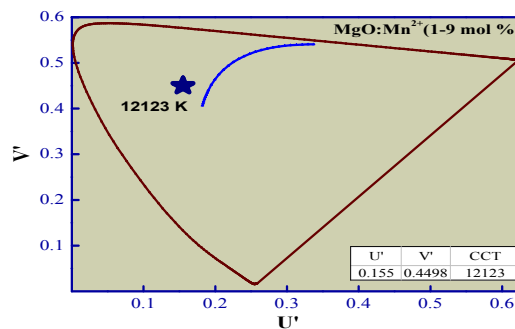

Fig.8(b). CCT diagram of MgO: Mn²⁺ (3 mol %) nanophosphor.

　　　　It was observed that the CIE co-ordinates of Mn^{2+} activated MgO: Mn^{2+} phosphor was very close to the National Television System Committee (NTSC) standard values, they fall close to the white region of chromaticity diagram and their corresponding location was marked with star in white region. Also, CCT was found to be 12123K using U'=0.155 and V'=0.4498. Therefore, the present phosphor was quite useful for the production of artificial white light to be similar to those of natural white light owing to its better spectral overlap in white LEDs and in solid state display applications.

4.　Conclusions

Low temperature solution combustion route was used for preparation of Mn^{2+} doped MgO blue-emitting phosphors. The PXRD results evident that simple cubic phase. SEM micrographs indicate that, the prepared samples were agglomerated from few microns to a few tens of microns, fluffy and porous in nature. The blue emission peak, observed at 405 nm was due to $^{3}B_{1u} \rightarrow {}^{1}A_g$ transition from Mn^{2+}ions.

　　Low temperature solution combustion route was used for preparation of Mn^{2+} doped MgO blue-emitting phosphors. The PXRD results evident that simple cubic phase. SEM micrographs indicate that, the prepared samples were agglomerated from few microns to a few tens of microns, fluffy and porous in nature. The IR studies confirms that the peaks were due to MgO. The blue emission peak, observed at 405 nm was due to $^{3}B_{1u} \rightarrow {}^{1}A_g$ transition from Mn^{2+} ions. Further, the excellent CIE chromaticity co-ordinates (x=0.2432, y=0.3138) which were very close to NTSC standard values of Blue color. Hence, MgO: Mn^{2+} (1-9 mol %) nanophosphor was promising material for optical display system applications.

TABLE 1. Calculated crystallite size values.

Mn^{2+} concentrations (mol %)	Crystallite size (nm)
0	7.7
1	7.4
3	6.5
5	6.3
7	5.3
9	5.1

References

1.　*Ramachandra Naik, Prashantha, S.C., Nagabhushana, H., Nagaswarupa, H.P, Anantharaju, K.S, Sharma, S.C, Nagabhushana, B.M., Premkumar, H.B., Girish, K.M, J. Alloys Compd. 617 (2014) 69-75.*

2.　*P.B. Devaraja, D.N. Avadhani, S.C. Prashantha, H. Nagabhushana, S.C. Sharma,B.M. Nagabhushana, H.P. Nagaswarupa, H.B. Premkumar. Spectr. Acta Part A: Molec. Biom. Spectr. 121 (2014) 46–52.*

3.　*P.B. Devaraja, D.N. Avadhani, S.C. Prashantha, H. Nagabhushana, S.C. Sharma, B.M. Nagabhushana, H.P. Nagaswarupa, Spectr. Acta Part A: Molec. Biom. Spectr.118 (2014) 847,851.*

4.　*V.R. Orante-Barro, L.C. Oliveira, J.B. Kelly, E.D. Milliken, G. Denis, L.G. Jacobsohn, J. Puckette, E.G. Yukihara, J. Lumin. 131 (2011) 1058–1065.*

5.　*L.C. Oliveira, E.D. Milliken, E.G. Yukihara, J. Lumin. 133 (2013) 211–216.*

6.　*[6] S. Azzaza, M. El-Hilo, S. Narayanan, J. Judith Vijaya, N. Mamouni, A. Benyoussef, A. El Kenz, M. Bououdina., Mat. Chem and Phy. 143 (2014) 1500-1507.*

7.　*M.M. Shang, D.L. Geng, Y. Zhang, G.G. Li, D.M. Yang, X.J. Kang, J. Lin, J. Mater. Chem. 22 (2012) 19094-19104.*

8. K.C. Patil, M.S. Hegde, Tanu Rattan, S.T. Aruna, "Chemistry of Nanocrystalline Oxide Materials, Combustion Synthesis, Properties and Applications", World Scientific Publishing Co. Pt. Ltd., UK, 2008.

9. Zhang Fen, Tang Wanjun, Opt. Mat. 37 (2014) 561–566.

10. P. Klug, L.E. Alexander, X-ray Diffraction Procedure, Wiley, New York, 1954.

11. Malleshappa, J., Nagabhushana, H., Sharma, S.C., Prashantha, S.C., Dhananjaya, N., Shivakumara, C., Nagabhushana, B.M. (2014). J. Alloy. Compd. 612, 425-434.

12. S.M. Borghei, S. Kamali, M.H. Shakib, A. Bazrafshan, M.J. Ghoranneviss, J. Fusi. Ener. 30 (2011) 433-436.

13. A. Kumar, S. Thota, S. Varma, J. Kumar, J. Lumin. 131 (2011) 640.

14. Y. Hao, G. Meng, C. Ye, X. Zhang, L. Zhang, J. Phys. Chem. 109 (2005)11204.

15. C.M. Janet, B. Viswanathan, R.P. Viswanath, T.K. Varadarajan, J. Phys. Chem. C 111 (2007) 10267.

16. A. Peter, Telex, J.R. Waldron, "Reflectance of Magnesium Oxide", J. Opti Soci of Amer. 45 (1955) 19-19.

17. S.Y. Yang, S.G. Kim, Powd. Tech. 146 (2004) 185-192.

18. S. Shi, M. Hossu, R. Hall, W. Chen, J. Mater Chem. 22 (2012) 23461-23467.

19. Oleg Viagin., Andrey Masalov., Irina Ganina., Yuriy Malyukin, Opt. Mat. 31 (2009) 1808-1810.

20. Xiang Ying Chen., Chao Ma., Zhong Jie Zhang., Xiao Xuan Li. Micropo. and Mesopo. Mat. 123 (2009) 202-208.

21. G. Blasse, A. Bril. Applied Physics Letter, 11 (1967) 53-55.

22. G. Blasse. Energy transfer in oxidic phosphors. Philips research reports, 24 (1969) 131-144.

23. L.G. an Uitert, J. Electro chem. Soc. 114 (1967) 1048-1053.

24. Z. Wang, P. Li, Z. Yang, Q. Guo, J. Lumin. 132 (2012) 1944-1948.

25. D.V. Sunitha, C. Manjunatha, C.J. Shilpa, H. Nagabhushana, S.C. Sharma, B.M. Nagabhushana, N. Dhananjaya, C. Shivakumara, R.P.S. Chakradhar, Spectr. Acta Part A: Molec. Biom. Spectr. 99 (2012) 279-287.

26. H.B. Premkumar, H. Nagabhushana, S.C. Sharma, S.C. Prashantha, H.P. Nagaswarupa, B.M. Nagabhushana, R.P.S. Chakradhar. (2014). J. Alloy .Compd, 601, 75-84.

27. Judd, B. Deane, Estimation of Chromaticity Differences and Nearest Color Temperature on the Standard 1931 ICI Colorimetric Coordinate System.